3D SEISMIC PHYSICAL MODELING FOR AZIMUTHAL VARIATIONS OF P-WAVE VELOCITY

Khaled Al Dulaijan, Gary F. Margrave, and Joe Wong

ABSTRACT

Information related to fracture orientation and intensity is vital for the development of unconventional hydrocarbons, such as tight sand gas and shale gas. Numerical modeling provides a valuable tool for geophysicists to test and validate their methodologies that provide them with information about reservoirs. Fractures make numerical modeling more complicated and introduce complexities that might even require geophysicists to validate their numerical models before using them to assess their methods. Alternatively, physical modeling provides a unique opportunity to test, validate, and develop methods for characterizing fractured reservoirs. This report utilizes seismic physical modeling to test a method for Velocity Variations with Azimuth (VVAz) for 3D seismic based on the non-hyperbolic NMO equation for TI media that was derived by Grechka and Tsvankin (1998).

A three-layer model was built using vertically laminated Phenolic overlain by Plexiglas to represent a fractured reservoir overlain by an isotropic overburden. HTI planes of phenolic have an orientation in northern half of the model that is orthogonal to HTI planes in southern half. A third layer of water is added to the model. 3D seimis data is acquired in patches. The data are processed and deconvolved with surface-consistent true relative amplitudes so they can be used for amplitude analysis. The third reflector, in the CDP domain, is very weak due to attenuation of anisotorpic phenolic and low fold of data. After sectoring the data, orientation and intensity of anisotropy is estimated by VVAz. Results of anisotropy orientation matches the physical model.

INTRODUCTION

Understanding fracture orientation and intensity is often challenging, yet important for the optimal development for fractured reservoirs. Fractures can act as conduits for fluid flow. Seismic anisotropy can assist in understanding fractures, even though sometimes it is related to the regional stress regime. In this report, we are interested in fracture-induced seismic anisotropy, and more specifically in vertical fractures or Horizontal-Transverse Isotropy (HTI). Azimuthal anisotropy makes numerical modeling difficult and introduces uncertainties in the numerical results. On the other hand, physical modeling provides a reliable alternative. This report is a continuation to previous CREWES work (e.g. Wong et al., 2012; Mahmoudian, 2013; Al Dulaijan et. al., 2014) that utilizes physical modeling, and is an in-progress work. Mahmoudian (2013) and Al Dulaijan et. al. (2014) have drawn conclusions about the stiffness coefficients of phenolic medium. Those conclusion were used in this report.

A three-layer model was built using vertically laminated Phenolic overlain by Plexiglas to represent a fractured reservoir overlain by an isotropic overburden. HTI planes of phenolic have an orientation in northern half of the model that is orthogonal to HTI planes

in southern half. A third layer of water is added to the model. The physial model is shown by Figure 1. Notice that the two layers of phenolic will not affect only traveltimes and amplitude, but also act as a fault in CDP time stacks as can be seen later.

In order to use the data for velocity and amplitude variations with azimuth, we implemented a standard 3D processing workflow described in this report. We faced and addressed several challenges to image the bottom of the Phenolic; these challenges wre due to three reasons:; 1. Fold was not large enough, 2. Phenolic generates very strong mode-converted PS waves, and 3. Phenlic is attenuative.

SEISMIC DATA ACQUISTION AND PROCESSING

The 3D seismic data was acquired over the physical model shown in Figure 1. The laboratory to field scale is 1:10,000 in both length and time. Scaled thicknesses of the three layers are: 300 m, 510 m, and 650 m. 3D seismic data were acquired over a scaled area of 4,000 m^2. Piezopin transducers were used as P-wave sources and receivers, with a central frequency at 2.38 MHz. Source and receiver transducers were positioned with a robotic system that has an error of less than 0.1 mm in laboratory scale. Just like conventional 3D seismic acquisition, data was acquired in patches. For each shot, 10 receivers were alive with a specific maximum offset. Receiver lines are east to west and have spacing of 50 m. Source lines are north to south and have spacing of 100 m. Source and receiver spacings are 100 m and 50 m respectively.

Data specifications, described above, yields a fold and azimuth distribution that is shown by Figure 2. Color indicates fold of 50 m x 25 m bins. High fold zone is indicated by red where fold is 120. Lower histogram indicates the azimuth distribution from -90º to 90º with reference to the north (*y*-axis). Figure 3. shows a shot gather with 10 receiver lines, and three main reflectors indicated. The three main reflectors are top of plexiglass, top of phenolic and base of phenolic. Notice that third reflector can barely been seen. Our target is the anisotropic layer between the second and third reflector.

For Amplitude Variations with Azimuth (AVAz) we are interested in the second reflector which is strong and there should not be an issue. On the other hand for Velocity Variations with Azimuth (VVAz), we are interested in the third reflector which is very weak because P waves have to travel through the phenolic layer twice. The phenolic layer is observed to create very strong mode-converted waves (Al Dulaijan et. al., 2014). Also, it is P-wave attenuative. One solution to these issues is to increase the fold that can be achieved only by acquisition. In this report, attempts to overcome the issues caused by inadequate spatial sampling are made by processing in time-domain and involve two main steps:

1. A common-offset stack for a complete half of the model where anisotropy orientation is known to be constant.

2. An FK filter designed to attenuate PS mode-converted waves.

A spherical divergence correction was were applied, as shown by Figure 3. Then, surface-consistent amplitude scaling was calculated and applied. Four scalers (source, receiver, offset, and CDP) were specifically calculated and applied. A surface-consistent deconvolution was applied, followed by another pass of surface-consistent amplitude. Figure 4 shows a shot gather before and after the application of surface-consistent amplitude and deconvolution, while corresponding amplitude spectra are shown by Figure 5. From the gather and spectra, we can see that higher frequencies are boosted and the amplitude spectrum is getting flatter over the data frequency band.

Velocity analysis was done by creating semblance coherency of super gathers. The maximum semblance (stacking response) were picked manually as shown by Figure 6. Figure 6 also shows the super gather after applying the picked NMO velocities. NMO corrections were applied to all CDP sorted data and stacked. Figure 7 shows a N-S inline (top) and E-W crossline (bottom). The three strong reflectors are: top of plexiglas, top of phenolic and bottom of phenolic. HTI planes of phenolic have an orientation in northern half of the model that is orthogonal to HTI planes in southern half. CMP stacks are created using isotropic NMO velocities. From the geometry of the model, crosslines are always parallel to HTI planes. Crosslines are perpendicular to HTI planes in southern half of the model, as can be seen by the third reflector (bottom of phenolic). That seam can be considered as a fault, as well, in CDP stack time domain. If non-hyperbolic NMO, or anisotropic time migration, had been applied, then the seam might be unnoticeable.

VELOCITY VARIATIONS WITH AZIMUTH

Grechka and Tsvankin (1998) showed that azimuthal variations of NMO velocities can be estimated by an ellipse in the horizontal plane under four assumption. First, the medium is arbitrarily anisotropic and inhomogeneous, so the azimuthal variations in traveltimes are smooth function of surface locations. Second, traveltimes exist at all azimuth. A case of salt domes creating a shadow zone at a specific azimuth violates the second assumption. A third assumption, routinely assumed in seismic data processing steps, such as CMP binning and stacking, is that traveltimes can be described by a Taylor series expansion of $t^2 x_\phi^2$, where t and x_ϕ are traveltime and source-receiver offset at specific azimuth. Lastly, traveltimes increase with offset at all azimuths. Those assumptions are nonrestrictive in most cases. Grechka and Tsvankin (1998) derived an elliptical NMO equation for TI media where source-receiver offset do not exceed the depth of the reflector. Hyperbolic NMO can be approximated by:

$$T^2 = T_0^2 + \frac{x^2}{V_{NMO}^2(\phi)} \tag{1}$$

, where

$$\frac{1}{V_{NMO}^2(\phi)} = \frac{1}{V_{slow}^2} cos^2(\phi - \beta_s) + \frac{1}{V_{fast}^2} sin^2(\alpha - \beta_s), \tag{2}$$

where T is the total two-way traveltimes, T_0 is the zero-offset two-way traveltimes. x is the offset, V_{fast} and V_{slow} are the fast and slow NMO velocities respectively. β_s is the azimuth of the slow NMO velocity, while $V_{NMO}(\phi)$ is the NMO velocity as function of the source-receiver azimuth (Figure 8).

Equation (2) can be written as:

$$\frac{1}{V_{NMO}^2(\phi)} = W_{11}\cos^2(\phi) + 2W_{12}\cos(\phi)\sin(\phi) + W_{12}\sin^2(\phi), \quad (3)$$

where W_{11}, W_{12}, and W_{22} are the ellipse coefficients that are related to the slow and fast NMO velocities and to the azimuth of the slow NMO velocity by

$$\frac{1}{V_{fast}^2} = \frac{1}{2}[W_{11} + W_{22} - \sqrt{(W_{11} - W_{22})^2 + 4W_{12}^2} \quad (4)$$

$$\frac{1}{V_{slow}^2} = \frac{1}{2}[W_{11} + W_{22} + \sqrt{(W_{11} - W_{22})^2 + 4W_{12}^2} \quad (5)$$

$$\beta_s = \tan^{-1}\frac{W_{11} - W_{22} + \sqrt{(W_{11} - W_{22})^2 + 4W_{12}^2}}{2W_{12}} \quad (6)$$

The azimuth of the fast velocity is 90º away from the azimuth of the slow velocities as shown by Figure 8 (Jenner, 2001). The total travel can be written as:

$$T^2 = T_0^2 + x^2\cos^2(\phi)W_{11} + 2x\,cos(\phi)\sin(\phi)W_{12} + x^2\sin^2(\phi)W_{22}. \quad (7)$$

Equation (7) can be written as:

$$d = Gm\,,$$

where *d* is n-dimensional data vector, *m* is the 6-dimensionl model parameter vector, and *G* is the n-by-4 data kernel as:

$$\begin{pmatrix} T_1^2 \\ T_2^2 \\ \vdots \\ T_n^2 \end{pmatrix} = \begin{pmatrix} 1 & x_1^2\cos^2(\phi_1) & 2x_1\,cos(\phi_1)\sin(\phi_1) & x_1^2\sin^2(\phi_1) \\ 1 & x_1^2\cos^2(\phi_1) & 2x_1\,cos(\phi_1)\sin(\phi_1) & x_1^2\sin^2(\phi_1) \\ \vdots & \vdots & \vdots & \vdots \\ 1 & x_{n1}^2\cos^2(\phi_n) & 2x_1\,cos(\phi_1)\sin(\phi_1) & x_1^2\sin^2(\phi_1) \end{pmatrix}\begin{pmatrix} T_0^2 \\ W_{11} \\ W_{12} \\ W_{22} \end{pmatrix}. \quad (8)$$

The resolution matrix (*N*) measures how well the data kernel resolves the model parameter. It is calculated by

$$N = GG^{-1} \tag{9}$$

and is shown in Fig. 9.

Because the bottom of phenolic reflection is very weak, we have created a common-offset stacks for the two halves of the model where the anisotropy orientation of the phenolic is constant. To strengthen the energy of the third reflector, we have also designed and applied an FK filter in attempt to attenuate the strong PS mode-converted waves. Figure 10 shows a common-offset stack of all azimuths: before (left) and after (right) application of FK filter for the attention of PS mode-converted wave at top of the phenolic. The reflector is significantly improved at time 1140 ms and near offset. Prior to stacking offset bins, the data were sectored every 30° from -90° to 90°. Figure 11 shows two common-offset stacks: 0° sector (left) and ± 90° (right). Also, picks of the bottom of the phenolic is indicated by red. Those time picks at different azimuths form the data vector in equation (8).

RESULTS

The VVAz method described above is applied to sectored azimuthal common-offset gathers. Zero-offset two-way traveltimes (T_0) obtained by VVAz is displayed for both halves of the model in the second column of Table. 1. T_0 was calculated using interval velocities from Al Dulaijan et. al. (2014). For the phenolic layer, V_{33} was used because it describes P-wave velocity at normal incidence. We found the T_0 values for the northern half of the model to be very accurate. The azimuth of the slow RMS velocity, β_s, is accurate for both parts of the model. The slow and vast RMS velocities were obtained by VVAz and calculated as well. To calculate them, we have used V_{11} and V_{22}, from Al Dulaijan et. al. (2013), for the fast and slow RMS velocities respectively and the interval to RMS velocity relation:

$$V_{RMS}^2 = \sum_{i=1}^{n} \frac{V_i^2 \Delta t_i}{\Delta t_i}, \tag{10}$$

where *n* is the number of layers and equal to 3. *V* is the interval velocity. Fast and slow RMS velocities obtained by VVAz are more accurate for the north part of the model.

	T_0 from VVAz	β_s from VVAz	V_{slow} from VVAz	V_{fast} from VVAz	Aniso %	Actual β_s	Calc. T_0	Calc. V_{slow}	Calc. V_{fast}
North Half	1.1617	89.809	2454	2641.1	7.3	90	1.1616	2473.3	2764.7
South Half	1.1759	0.6368	2133.1	2623.2	20.6	0	1.1616	2473.3	2764.7

Table. 1. Comparison between VVAz results and calculated results

CONCLUSIONS AND FUTUREWORK

Physical modeling can be a valuable tool that to test and evaluate geophysical methods, especially for anisotropic media where numerical modeling becomes complicated and may require validation by experimental observations. For the study described in this report, a 3D pre-stack physical modeling dataset was acquired, processed and used to evaluate a method for analyzing VVAz. The most serious shortcoming in this study is that, because of inadequate spatial sampling during acquisition, there is not enough fold to overcome by normal processing the fact that the reflection of bottom of the phenolic layer is weak and contaminated by strong mode-converted PS waves generated by the top of the anisotropic layer. We devised an extra time-domain processing method to overcome this issue, and it was necessary to use it to advance the VVAz analysis of the physically-modeled data. Results of the analysis proved to very accurate for the north part of the model, and less accurate for the south part of the model.

We believe that the use of interval velocity has an advantage over the use of RMS velocities because it will make VVAz less sensitive to overburden properties. Therefore, we plan to improve our code by using a Dix-type formula to obtain interval NMO ellipses (Grechka et al., 1999). We plan to further use the data for Amplitude Variations with Azimuth AVAz using Rüger (2001) and Fourier coefficients to estimate fractures intensity and directions maps. We will apply these extended techniques to a new dataset to be acquired with increased spatial sampling (i.e., source and receive line spacings = 50m, source and receiver intervals = 50m along each line).

ACKNOWLEDGMENT

REFERENCES

Al Dulaijan, K., G. Margrave and J. Wong, 2014, Azimuthal anisotropy investigations for P and S waves: a physical modelling experiment: CREWES Research Report.

Grechka, V., & Tsvankin, I., 1998, 3-D description of normal moveout in anisotropic inhomogeneous media. Geophysics, 63(3), 1079-1092.

Jenner, E., 2001, Azimuthal anisotropy of 3-D compressional wave seismic data, Weyburn Field, Saskatchewan, Canada: Ph.D. thesis, Colorado School of Mines.

Mahmoudian, F., 2013, Physical Modeling and Analysis of Seismic Data from a Simulated Fractured Medium: Ph.D. thesis, University of Calgary.

Rüger, A., 2001, Reflection coefficients and azimuthal AVO analysis in anisotropic media. Society of Exploration Geophysicists.
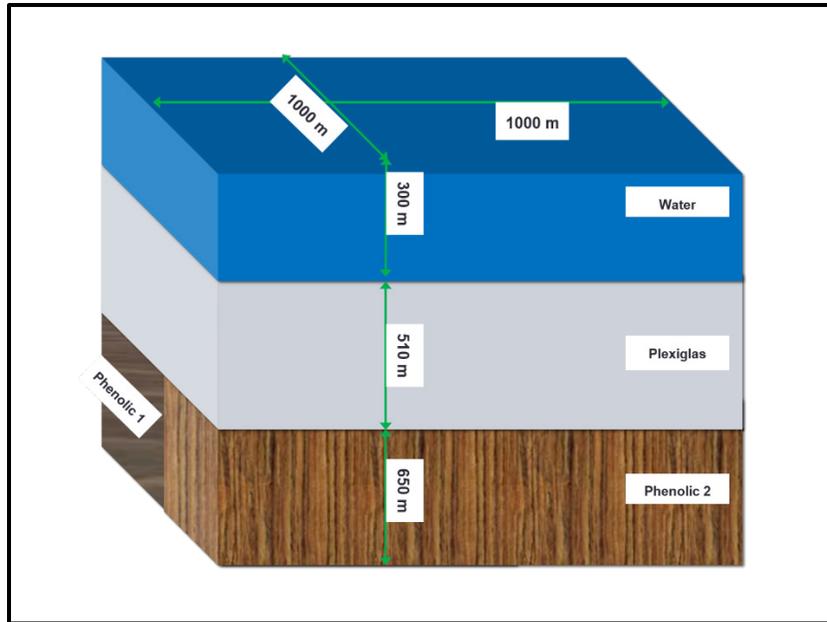
Fig. 1. A three-layer physical model. The model is constructed using vertically laminated Phenolic overlain by Plexiglas to represent a fractured reservoir overlain by an isotropic overburden. HTI planes of phenolic have an orientation in northern half of the model that is orthogonal to HTI planes in southern half. A third layer of water is added to the model. Laboratory to field scale is 1:10,000 in both length and time. Scaled thicknesses of the three layers are: 300 m, 510 m, and 650 m.
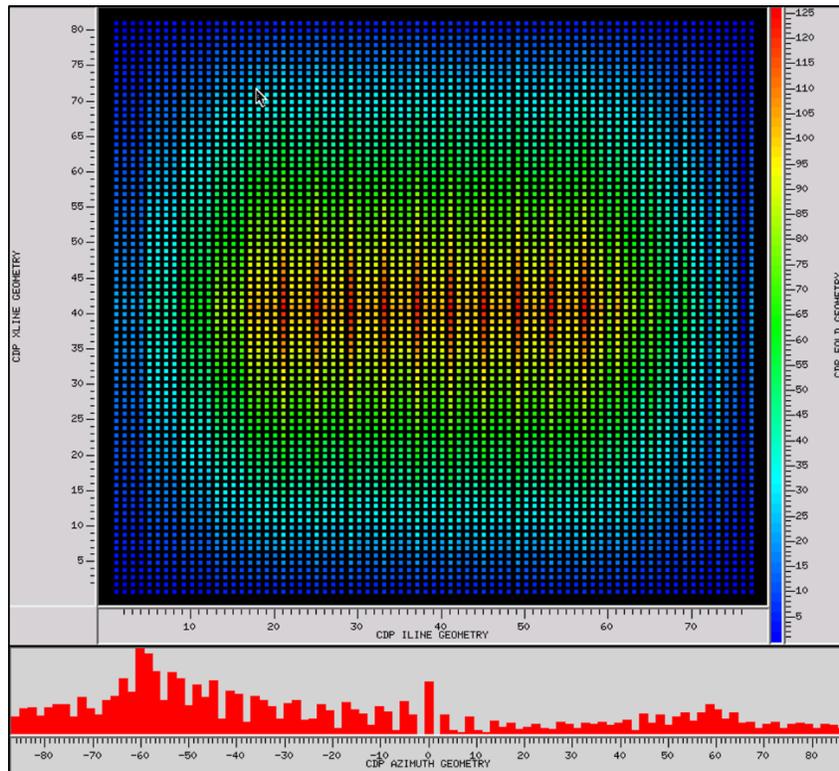

Fig. 2. A basemap for the 3D seismic physical modeling dataset. Color indicates fold of 50mx25m bins. High fold zone is indicated by red where fold is 120. Lower histogram indicates the azimuth distribution from -90° to 90° with reference to the north (*y*-axis).
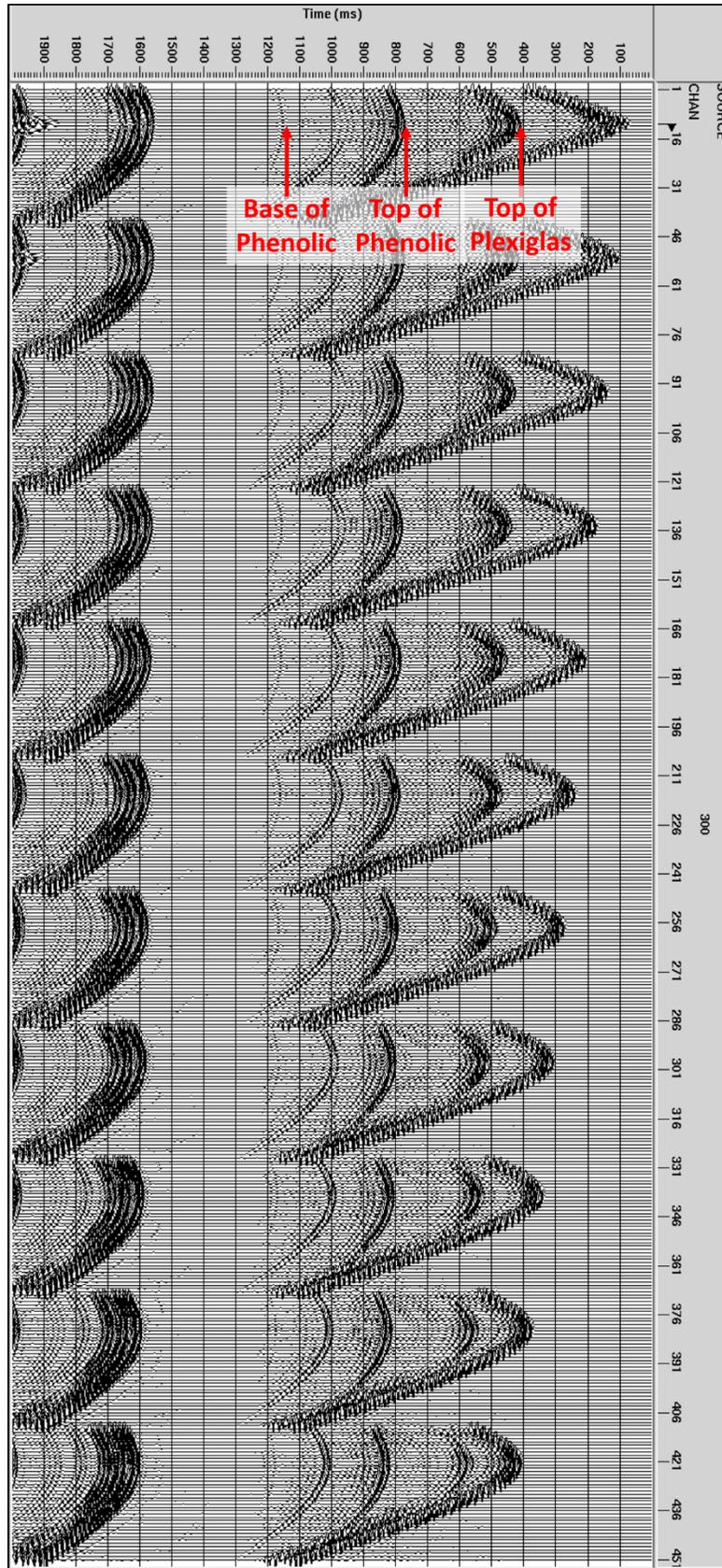
Fig 3. A shot gather: 10 reciever lines. Target is Phenolic, between 2nd and 3rd reflector.
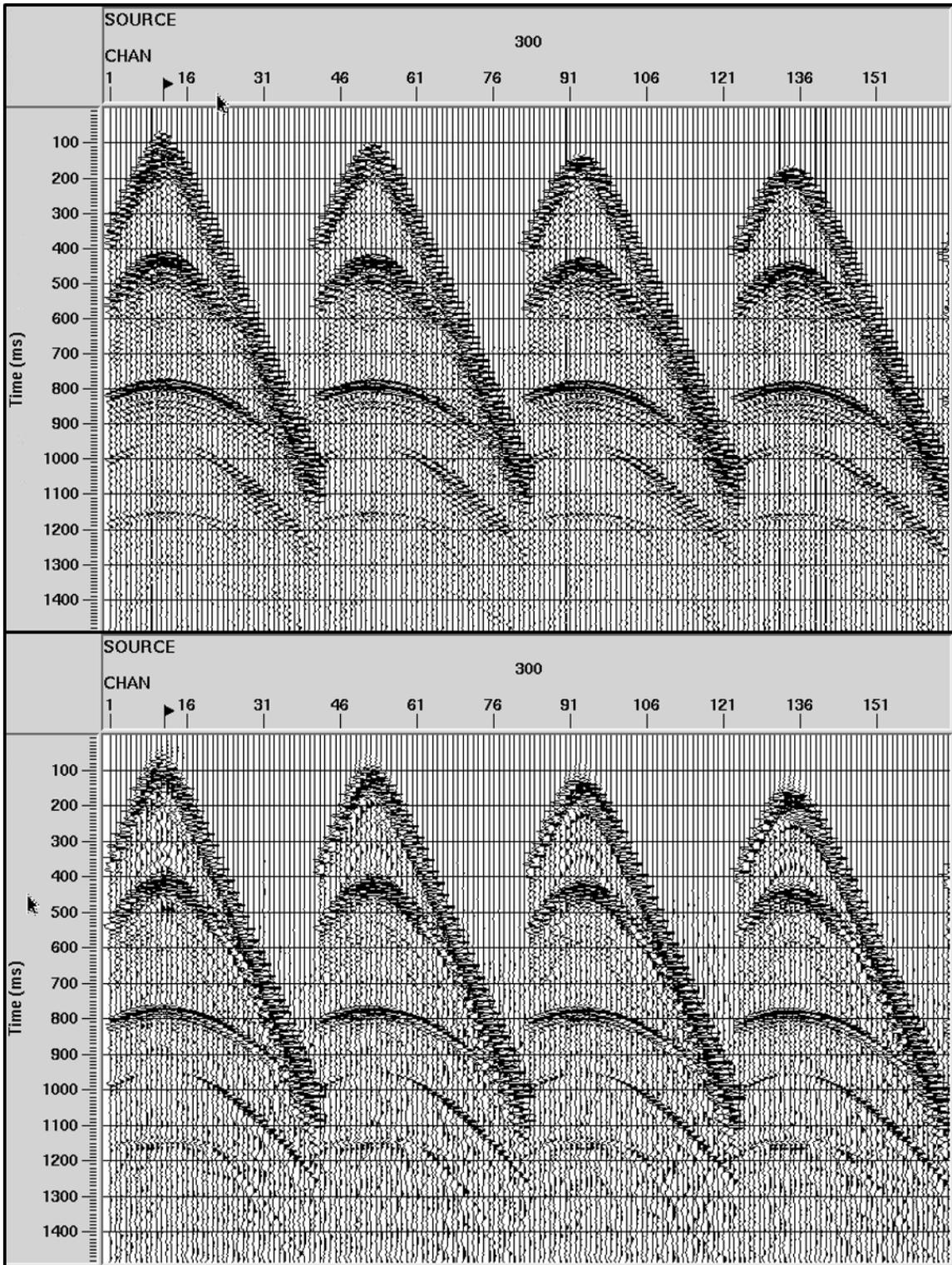
Fig 4. A shot gather: 4 out of 10 reciever lines are shown. Data is before applying surface-consitent amplitude scaling and deconvolution (top) and after applying surface-consistent amplitude scaling and deconvulion (bottom). Note the prominent PS arrivals with apexes at about 780ms.
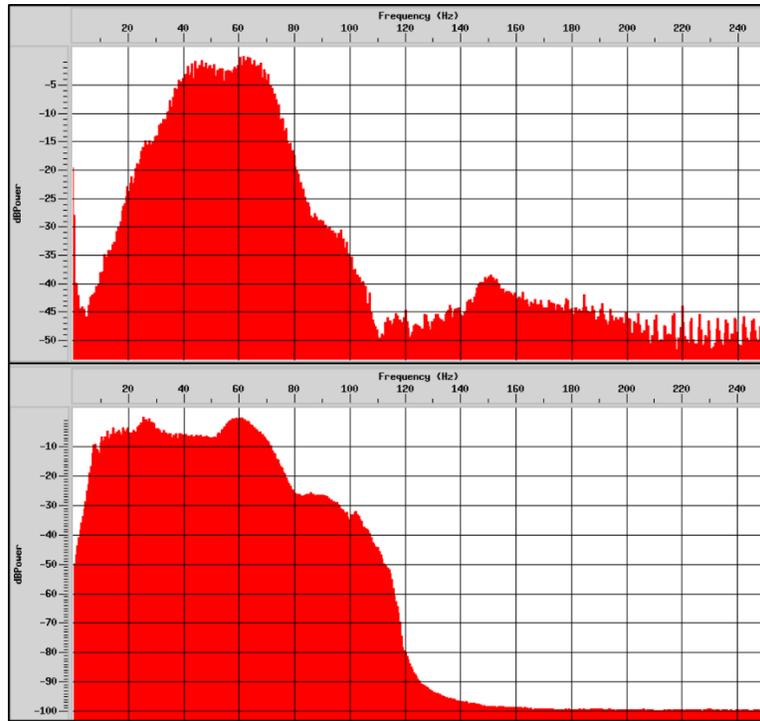
Fig 5. Ampiltud spectra: before deconvoluion (top) and after deconvultion (bottom).
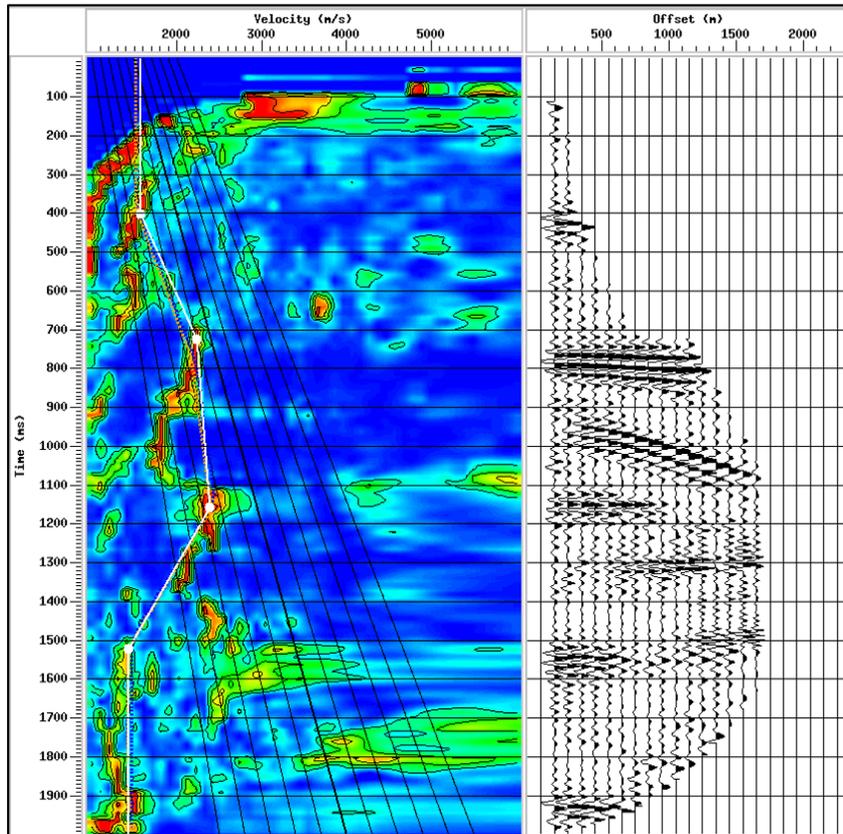
Fig. 6. Velocity analysis: A semblance coherency with picks of maximum stacking indicated by white dots (left) and CDP gather with flat reflection events (right).
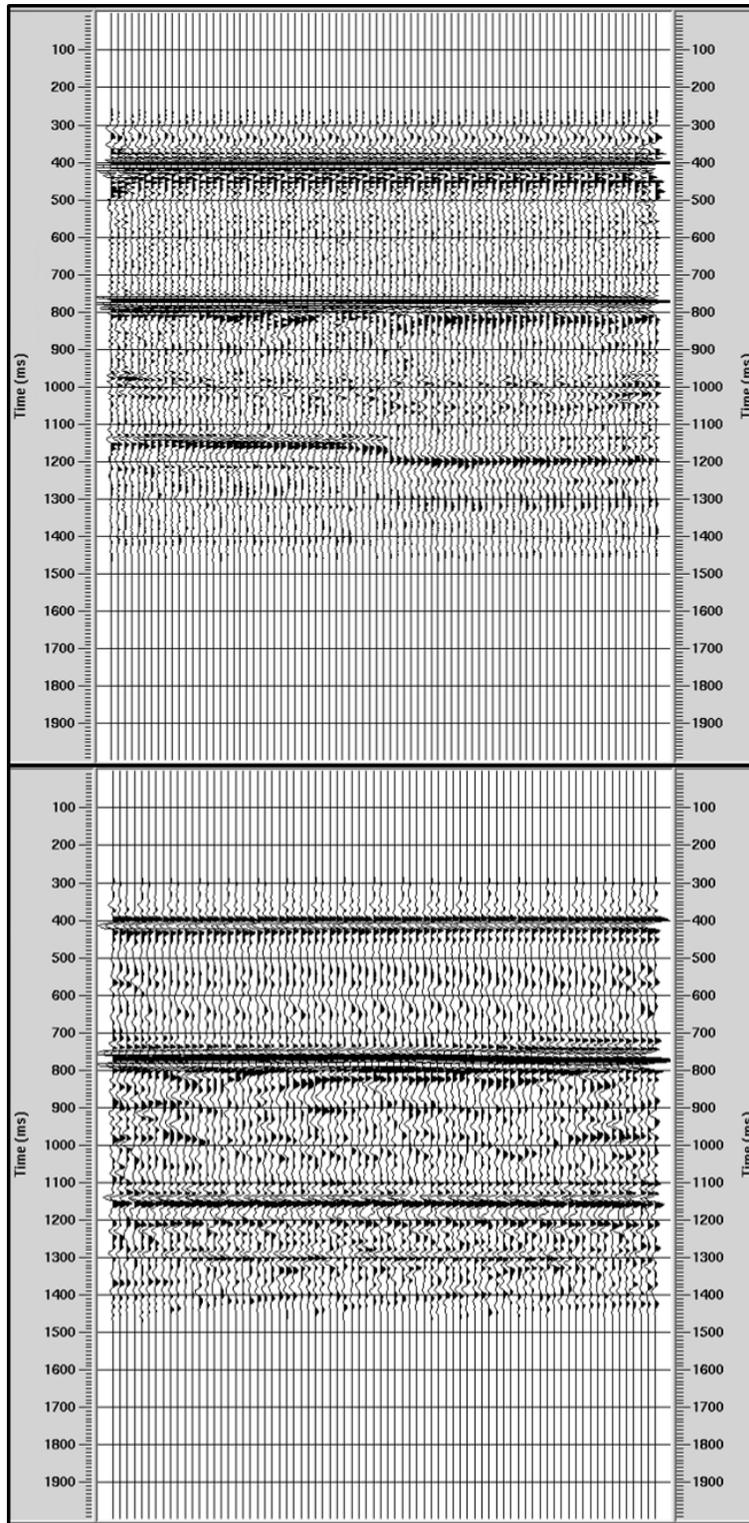
Fig 7. CDP Stacks: a N-S inline (top) and E-W crossline (bottom). The three strong reflectors are: top of plexiglas, top of phenolic and bottom of phenolic. HTI planes of phenolic have an orientation in northern half of the model that is orthogonal to HTI planes in southern half. CMP stacks are created using isotropic NMO velocities. From the geometry of the model, crosslines are always parallel to HTI planes in the northern half of the model. Crosslines are perpendicular to HTI planes

in southern half of the model, as can be seen by the third reflector (bottom of phenolic). That seam can be considered as a fault.
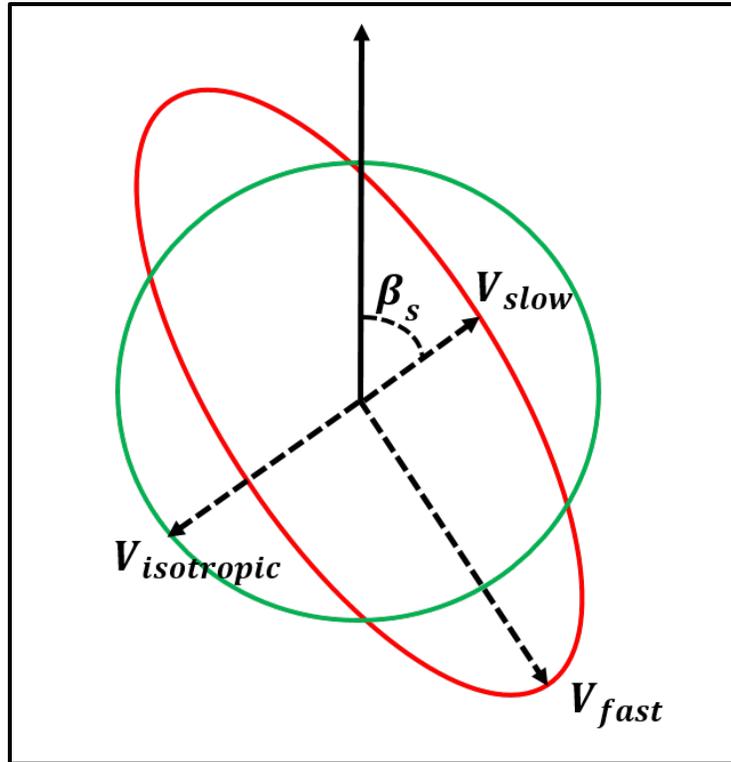

Fig. 8. Isotropic RMS velocity vs azimuthally variant RMS velocity.
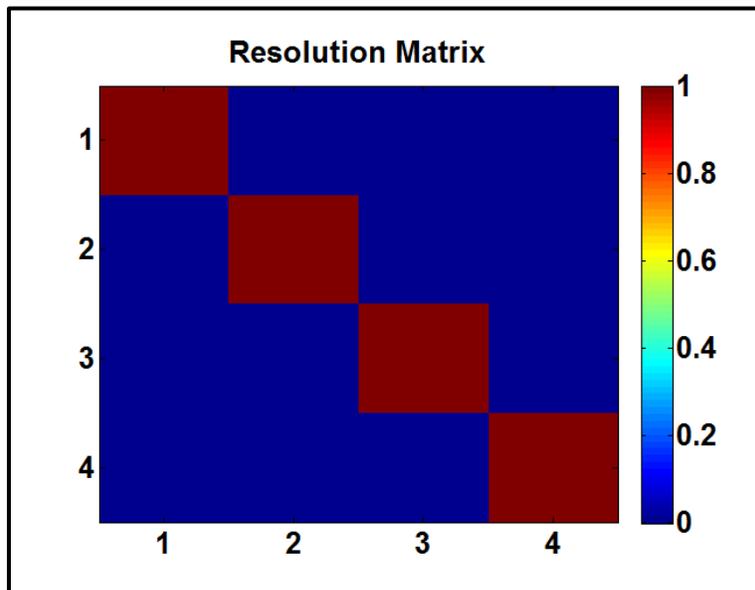
Fig. 9. The resolution matrix of the geometry of all offset and azimuth used for VVAz.
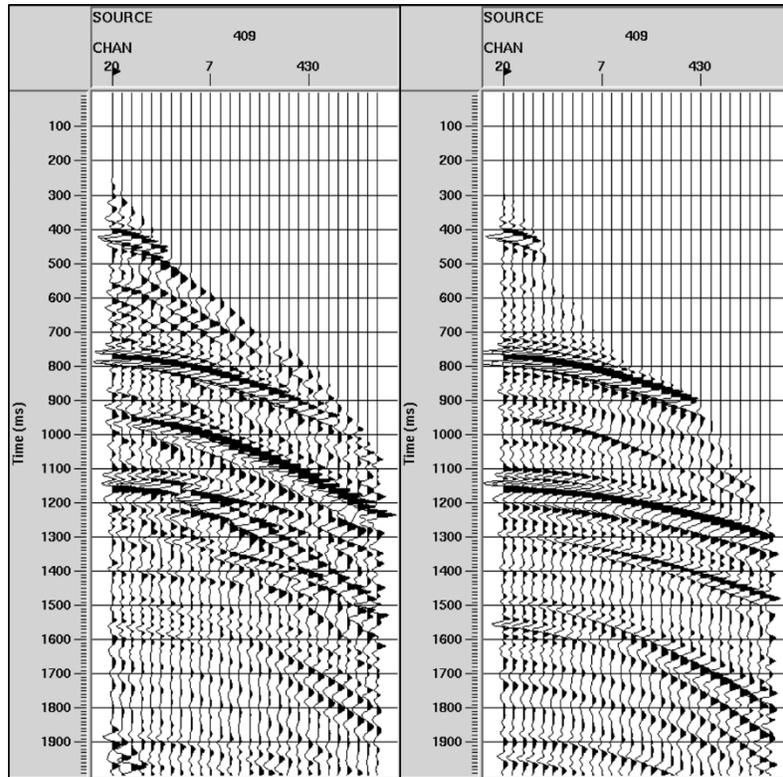
Fig 10. Common-offset stack of all azimuths: before (left) and after (right) application of FK filter for the attenuation of PS mode-converted wave at top of the phenolic. The reflector is significanly improved at time 1140 ms and near offset.
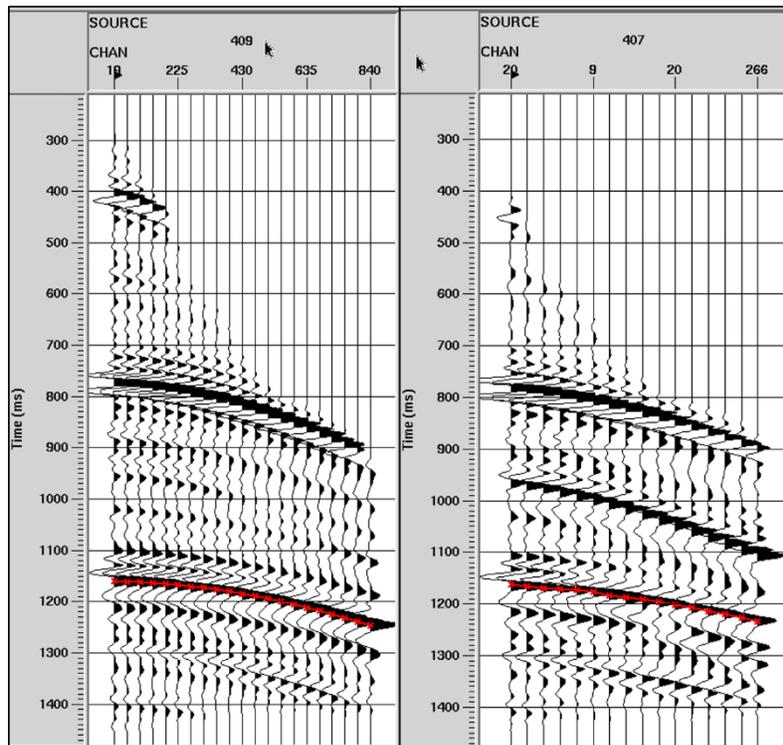

Fig. 11. Common-offset stacks with top of phenolic picks of 0º sector (left) and ± 90º (right).